Physics of Plasmas ARTICLE scitation.org/journal/php

Causality, intermittence, and crossphase evolution during confinement transitions in the TJ-II stellarator

Cite as: Phys. Plasmas **28**, 092302 (2021); doi: 10.1063/5.0057791
Submitted: 25 May 2021 · Accepted: 10 August 2021 ·
Published Online: 2 September 2021

B. Ph. van Milligen,[1,a)] B. A. Carreras,[2,3] I. Voldiner,[1] U. Losada,[1] C. Hidalgo,[1] and TJ-II Team[1]

AFFILIATIONS

[1]National Fusion Laboratory, CIEMAT, Avda. Complutense 40, 28040 Madrid, Spain
[2]Departamento de Física, Universidad Carlos III, Avda. de la Universidad 30, 28911 Leganés, Spain
[3]Department of Physics, University of Alaska, Fairbanks, 99775-5920 Alaska, USA

[a)]Author to whom correspondence should be addressed: boudewijn.vanmilligen@ciemat.es

ABSTRACT

In this work, we study spontaneous electron to ion root transitions in TJ-II using Langmuir probes. By scanning the probe position on a shot to shot basis, we reconstruct a spatiotemporal map of the evolution of important turbulent quantities in the plasma edge region. We pay particular attention to the evolution of the cross phase between transport-relevant variables, showing the spatiotemporal evolution of this quantity for the first time, revealing the outward propagation of the changes associated with the transition. We also compute the intermittence parameter, which allows us to conclude that the turbulence, although its amplitude increases, condenses in a reduced number of dominant modes and becomes less bursty. The causal relationship between variables is studied using the transfer entropy, clarifying the interactions between the main variables and offering a rather complete picture of the complex evolution of the plasma across the confinement transition.

I. INTRODUCTION

Fusion plasmas are strongly driven systems, exhibiting some of the steepest temperature gradients of all known systems, and are, therefore, far from thermodynamic equilibrium. These systems exhibit phase transitions (confinement transitions) in which order arises spontaneously out of strong turbulence in the form of zonal flows, associated with the establishment of a radial electric field and a transport barrier involving the modification of turbulence.[1] The complex interactions between radial transport (profiles) and turbulence remain a subject of intense study, in view of the importance of transport barriers for the efficiency and viability of putative fusion reactors. In this work, we study the regulation of transport by sheared flows through the cross phase between fluctuating variables,[2–5] with unprecedented spatiotemporal resolution, and use some advanced techniques [the transfer entropy (TE) and intermittence] to provide deeper insight into these processes.

This paper is organized as follows: Sec. II describes the experimental setup, Sec. III describes the methods that were used, and Sec. IV provides the experimental results. The results are discussed in Sec. V, and some conclusions are drawn in Sec. VI.

II. EXPERIMENTAL SETUP

TJ-II is a flexible Heliac[6] with toroidal magnetic field $B_T \simeq 1$ T, major radius $R_0 = 1.5$ m, and minor radius $a < 0.22$ m.[7] Plasmas can be heated using two Electron Cyclotron Resonance Heating (ECRH) beam lines delivering up to 300 kW each at a frequency of 53.2 GHz (X mode) and two Neutral Beam Injector (NBI) systems (co and counter) with up to 2×700 kW port-through power. The line average electron density is measured using a microwave interferometer.[8]

In this work, we analyze a set of similar ECR heated discharges with a magnetic configuration (labelled "100_46_65") characterized by low magnetic shear and a rotational transform $\iota(0) \simeq 1.575$ and $\iota(1) \simeq 1.665$. The vacuum configuration has some important rational surfaces in the edge region ($\iota = 5/3$ at $\rho \simeq 1$ and $\iota = 18/11$ at $\rho \simeq 0.86$). Since both plasma pressure and internal plasma currents are small, the actual magnetic configuration closely matches the externally imposed configuration.[9]

TJ-II is fitted with two reciprocating probe drives. Probe drive D (located at toroidal position $\phi = 38.2°$) is fitted with a staircase head containing three triple probes.[10,11] Each triple probe consists of three pins, measuring V_f, I_{sat}, and V_f, respectively, where V_f is the floating

potential and I_{sat} is the ion saturation current. Probe drive B (at $\phi = 195°$) is fitted with a rake probe, containing a triple probe at its tip and several radially distributed pins along its side.[12]

III. METHODS

The difference of the two V_f measurements of the triple probe, aligned poloidally, divided by their distance d_θ, provides an estimate of the poloidal electric field, E_θ, at the same location as the I_{sat} measurement. The sign convention of E_θ follows Ref. 13. Likewise, the radial electric field E_r can be estimated from the difference of two V_f signals divided by their radial distance d_r using two radially spaced probe pins.

The fluctuating particle flux Γ can be estimated from $\Gamma = \langle \tilde{n}\tilde{E}_\theta \rangle / B$. The ion saturation current I_{sat} is assumed proportional to the fluctuating density $\tilde{n}$. Thus, the fluctuating particle flux is proportional to the fluctuation amplitudes or root-mean-square values RMS (I_{sat}) and RMS (E_θ), as well as the cosine of the phase angle $\Delta\phi$ between these two quantities, cos ($\Delta\phi$).[1] Hence, these quantities play a major role in the understanding of particle transport and are the prime focus of this work.

The probe data also allow estimating the phase velocity v_θ using the two-point correlation technique[14] applied to the mentioned two poloidally aligned V_f signals. Thus, using this probe setup, a rather complete set of data are accessible to study turbulence evolution during confinement transitions.

The phase angle is estimated using two alternative techniques. The complex coherence $\gamma(f)$ of two signals $x(t)$ and $y(t)$ over a time window $T = \{t_0 \le t < t_1\}$ is calculated by subdividing this time window in a small number N of subwindows, calculating the complex Fourier transforms $X(f)$ and $Y(f)$ for each subwindow, and evaluating $\gamma = \langle XY^* \rangle_N / \sqrt{\langle |X|^2 \rangle_N \langle |Y|^2 \rangle_N}$. Here, $\langle \cdot \rangle_N$ denotes an average over the N subwindows. The frequency-averaged cross phase $\Delta\phi_{coh}$ of the coherence is estimated over a range of frequencies using $\exp(i\Delta\phi_{coh}) = \sum_f \gamma / \sum_f |\gamma|$.

Alternatively, the Hilbert cross phase is calculated for a time window T by calculating the fluctuating part of the signals, $\tilde{x}(t) = x(t) - \langle x \rangle_T$, where $\langle \cdot \rangle_T$ is the average over T and similar for y. Then, the Hilbert transform is applied to $\tilde{x}$ and $\tilde{y}$, yielding complex signals $\hat{x}(t)$ and $\hat{y}(t)$. The Hilbert cross phase $\Delta\phi_H$ is defined from $\exp(i\Delta\phi_H) = \langle \hat{x}\hat{y}^* \rangle_T / \sqrt{\langle |\hat{x}|^2 \rangle_T \langle |\hat{y}|^2 \rangle_T}$.

The intermittence parameter arises in the field of chaos theory.[15,16] The fluctuation level of a time series of length N is characterized by its normalized root-mean-square (RMS) value ϵ, calculated over subtime windows with length $n \le N$: $\epsilon = \mathrm{RMS}_n / \mathrm{RMS}_N$. The moments $\langle \epsilon^{\mathbb{q}} \rangle_n$, averaged over all available subwindows with length n, are expected to decay as a power of the window length, namely, $\langle \epsilon^{\mathbb{q}} \rangle_n \propto n^{-K(\mathbb{q})}$. Since we are interested in the turbulent (high frequency) characteristics of the fluctuations, we determine $K(\mathbb{q})$ from a linear fit of a set of values of $\log \langle \epsilon^{\mathbb{q}} \rangle$ vs $\log n$, for a range of values of $n = 1, \ldots, n_1$, where n_1 is small, e.g., $n_1 = 8$. When K is linear in $\mathbb{q}$, the time series is considered to be monofractal, otherwise it is multifractal. The intermittence parameter C_1 is defined as the derivative $dK/d\mathbb{q}$ evaluated at $\mathbb{q} = 1$ and ranges from 0 for a monofractal time series to 1 for a multifractal time series.[17] It is rather insensitive to random noise.[18] Signals with high value of C_1 are more "bursty" in nature than signals with low C_1.

The Transfer Entropy (TE) is a nonlinear analysis technique, related to the mutual information, that has proven useful for determining causal relations between fluctuating variables[19] and the study of heat transport in stellarators,[20] among others. It measures the "information transfer" between two time series $x(t_i)$ and $y(t_i)$ by quantifying the number of bits by which the prediction of the next sample of signal y can be improved by using the time history of not only the signal y itself, but also that of signal x. We use a simplified version of the transfer entropy that can be written as

$$T_{X\to Y} = \sum p(y_{i+1}, y_{i-k}, x_{i-k}) \log_2 \frac{p(y_{i+1}|y_{i-k}, x_{i-k})}{p(y_{i+1}|y_{i-k})}, \qquad (1)$$

where the p's are multidimensional probability distributions calculated from the data. Only a single historical value $(i-k)$ of x and y is used to determine the impact on the next value of y (at $i+1$). Thus, we compute $T_{X\to Y}$ for a range of values k to study the causal impact at various "time lags." If the prediction of the signal y is improved by the information contained in signal x, $T_{X\to Y}$ will be significant and there is a flow of information $x \to y$, which can be interpreted in the sense that x impacts y or has a causal influence on y. Unlike the mutual information and the standard linear correlation (which merely quantifies a similarity of waveform), this quantity is directional (from x to y), as would be required of any quantifier of causality. Even so, as with any quantifier of causality, one can never rule out the existence of a third (possibly undetected) variable z that affects both x and y, so the transfer entropy only provides an indication of causality and no proof.

IV. EXPERIMENTAL RESULTS

In TJ-II ECRH plasmas, when the line average electron density is raised above a critical value of $\overline{n_e} \simeq 0.6 \times 10^{19}$ m^{-3}, the plasma performs a spontaneous transition from electron root to ion root confinement.[21–23] Among other things, this transition is characterized by a change of sign of the radial electric field E_r in the edge region.

In the discharges analyzed here, these spontaneous confinement transitions were achieved repetitively and systematically by modulating the gas puff. In previous work, the global evolution of profiles (potential, density) and fluctuations from edge Langmuir probes were studied, and the formation of the edge particle transport barrier was visualized.[22] Magnetic activity was studied using Mirnov pickup coils and poloidal flow using Doppler reflectometry.[24] Heat transport was analyzed using electron cyclotron emission data in Ref. 20 and core intermittence using heavy ion beam probe data in Ref. 18.

Figure 1 shows some typical time traces. Apart from the top time trace (a), all data are obtained from the D probe system, located inside the plasma at $\rho \simeq 0.92$. The transition roughly occurs when the line average electron density $\overline{n_e}$, Fig. 1(a), crosses the value $\sim 0.6 \times 10^{19}$ m^{-3}. The root-mean-square fluctuation amplitude of the density time trace increases during the transition, as reported in previous work.[25]

Figure 1(b) shows that the smoothed floating potential (averaged over two poloidally spaced V_f probe tips) changes sign at the transition, as does the poloidal velocity v_θ shown in Fig. 1(c). Figure 1(c) also shows the smoothed radial electric field E_r. Assuming that the poloidal velocity is dominated by the $E \times B$ flow and considering that the TJ-II magnetic field $B \simeq 1$ T, the numerical values of E_r and v_θ should be very close, and so they are, except near the transition, where E_r appears to be affected by a strong zonal flow contribution. A zonal flow structure is poloidally and toroidally symmetric and, therefore,

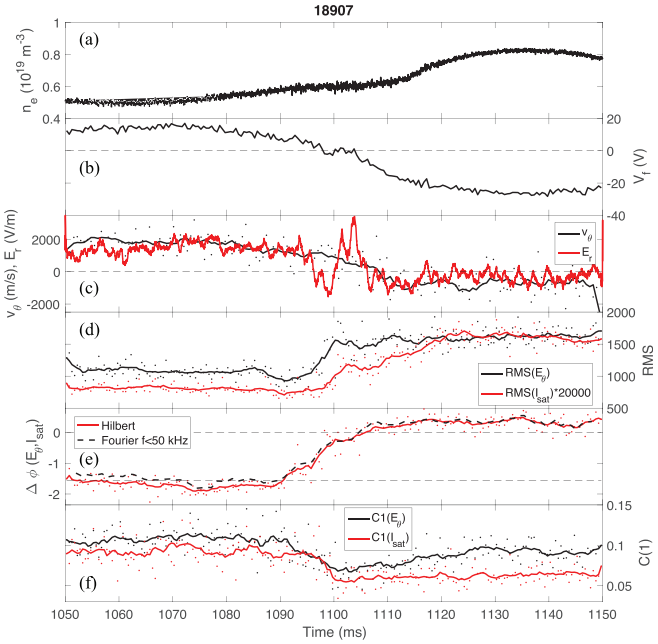

FIG. 1. Time traces of some relevant quantities across the e-root to i-root transition (configuration 100_46_65). The Langmuir probe position is $\rho \simeq 0.92$. Top to bottom: (a) the line integrated electron density $\overline{n_e}(10^{19}\ \mathrm{m}^{-3})$. (b) Running average of the floating potential V_f. (c) Poloidal velocity, computed from the two-point correlation technique using two poloidally spaced V_f pins and radial electric field calculated from two radially spaced V_f pins. (d) The RMS variation of E_θ (black) and I_{sat} (red) from the triple probe. (e) Cross phase between E_θ and I_{sat} calculated using two methods, as indicated in the legend. Horizontal dashed lines indicate multiples of $\pi/2$. (f) Intermittence of E_θ (black) and I_{sat} (red). In (c)–(f), dots are calculated values, and the same-colored line is a smoothed curve through the dots.

would not affect v_θ, which is derived from two poloidally displaced probe pins. This interpretation is reinforced by the fact that long range correlations[21] between the remote B and D probes have been detected around this time,[22] another hallmark of zonal flows.

Prior to the transition, the turbulence amplitude as quantified by the RMS values of E_θ and I_{sat} [shown in Fig. 1(d)] is roughly constant, but at $t = 1090$ ms, it significantly increases. Figure 1(e) shows that the cross phase between E_θ and I_{sat}, calculated using the two methods described above, gradually changes from about $-\pi/2$ for $t < 1090$ ms to ~ 0 for $t > 1110$ ms. Figure 1(f) shows that the intermittence parameter C_1 for these two quantities is roughly constant for $t < 1090$ ms and then significantly drops at $t \simeq 1100$ ms.

Figure 2 shows the spectrogram of E_θ for the discharge shown in Fig. 1. It shows an increase in low-frequency activity following the transition, consistent with the increase in RMS (E_θ). The very low frequency activity ($f < 10$ kHz) is particularly intense around the time of the transition and is presumed to be related to the mentioned zonal flow. The later, higher frequency activity ($20 < f < 30$ kHz) is known to be related to a rotating MHD mode, as reported in Ref. 24 on the basis of Mirnov coil analysis.

In this discharge, the B probe was located at approximately the same radial position ($\rho \simeq 0.9$) as the D probe. One of the pins of the B probe was setup to measure T_e using the fast swept probe technique.[26] Results are shown in Fig. 3. It is observed that the electron

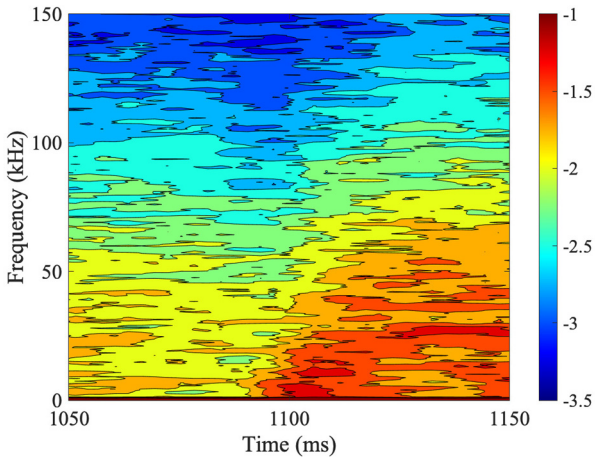

FIG. 2. Spectrogram of E_θ for discharge 18907 (cf. Fig. 1). The color bar specifies the value of $\log_{10}(S^2)$, where S^2 is the spectral power.

temperature slightly increases following the transition, but can be discarded as the cause of the observed phase changes.

Probe B was radially moved on a shot to shot basis. This allows obtaining not only the temporal, but also the spatial variation of many quantities. To compare discharges with slightly varying transition times, we defined a critical time t_{crit} as the time at which v_θ changes sign and then displayed the quantities as a function of $t - t_{crit}$.

Results are shown in Fig. 4. The vertical axis shows the position of probe B in each shot (in terms of the normalized minor radius, ρ). Colors indicate the value of the quantity shown above each panel.

Figures 4(a) and 4(b) show the evolution of the RMS fluctuation amplitude of I_{sat} and E_θ. Both significantly increase following the transition, more strongly so in the inner half ($\rho \lesssim 0.93$) of the examined region. Figures 4(c) and 4(d) show the intermittence of I_{sat} and E_θ. It decreases after the transition, mainly in the same region where the fluctuation amplitude increases.

Figure 4(e) shows the cross phase between E_θ and I_{sat}, calculated using the coherence technique (integrating over frequencies <50 kHz). At small values of $\rho \lesssim 0.91$, the phase increases from around $-\pi/2$ to

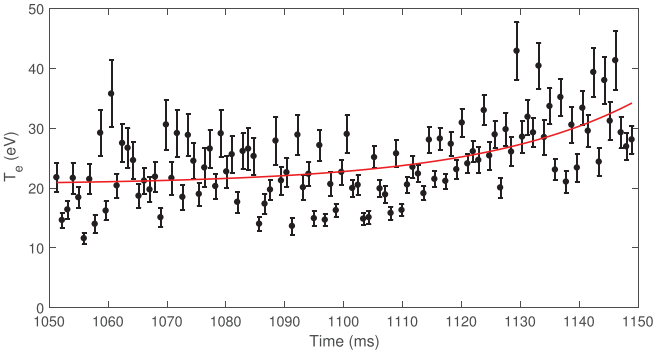

FIG. 3. Electron temperature evolution at $\rho \simeq 0.9$ for the same discharge as Fig. 1, computed using the swept probe technique. Error bars correspond to the 1σ confidence level of the $I_{sat}(V_s)$ fit (see the text).

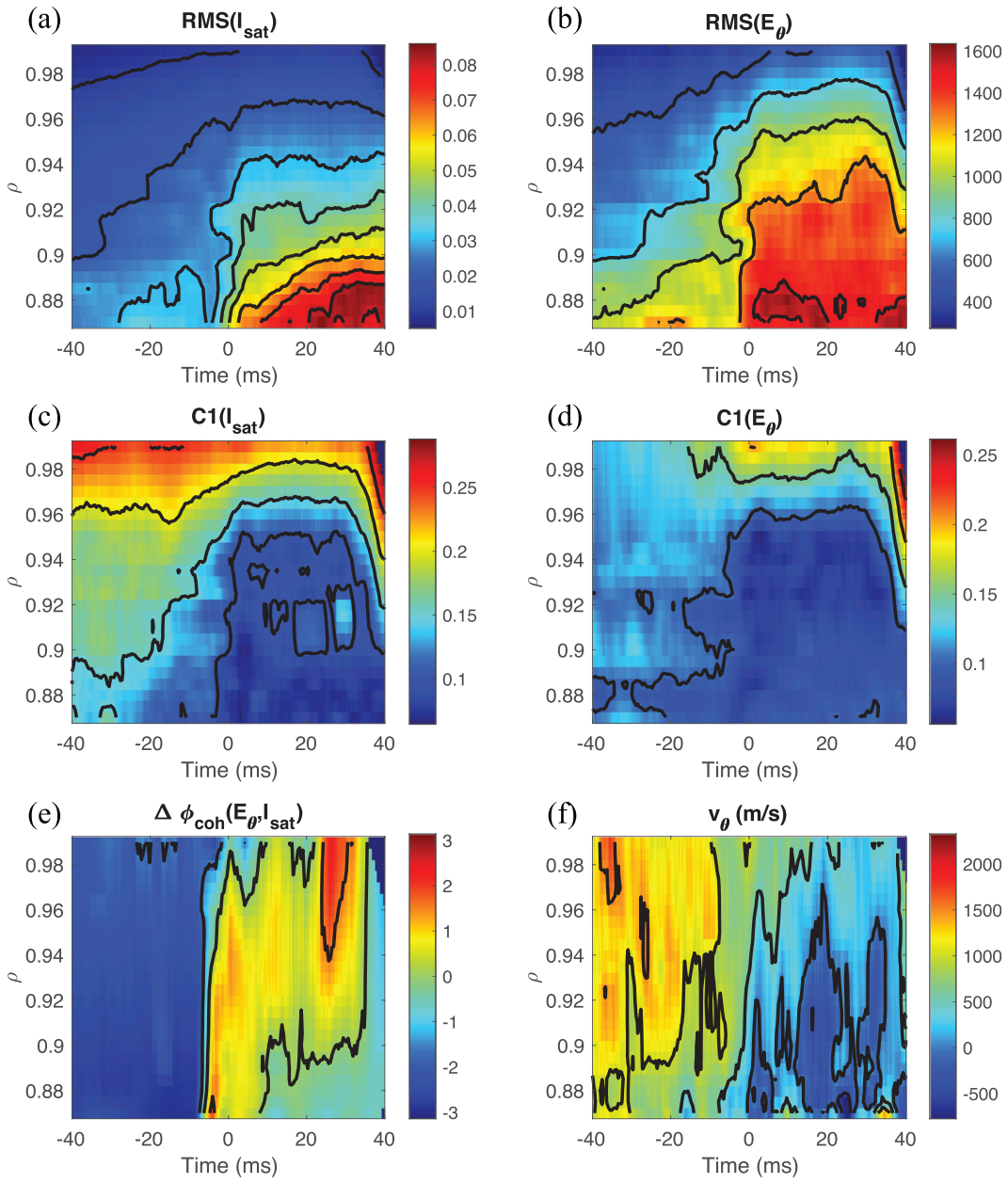

FIG. 4. Spatiotemporal evolution of some relevant quantities across the e-root to i-root transition (configuration 100_46, probe B). The ρ coordinate corresponds to the position of probe B in each discharge. The horizontal axis shows the time minus the critical time (see the text).

~ 0 or less across the transition. At larger values of ρ, the phase increases even more, similar to Fig. 1 (probe D), and reaches values $>\pi/2$ at the outermost positions. Black contours are drawn at multiples of $\pi/2$ to facilitate understanding. Before the transition, the radial phase profile is almost flat, but after the transition strong radial variation exists, such that the cross phase is maximal near $\rho \simeq 0.96$ and minimal near $\rho \simeq 0.88$. In the region of the transport barrier ($\rho \simeq 0.95$), the temporal variation of the RMS is only mild, whereas the temporal variation of the cross phase is very significant.

Figure 4(f) shows the poloidal phase velocity, calculated using the two-point correlation technique. It evolves from positive to negative across the transition, similar to Fig. 1, although values differ according to radius. The configuration of this probe did not allow calculating E_r.

From previous work, it is known that the line average electron density $\overline{n_e}$ plays the role of a control parameter for spontaneous confinement transitions at TJ-II.[10] Figure 5 shows the Transfer Entropy (TE) between this parameter and various relevant quantities at different time lags (horizontal axis). It should be remembered that the

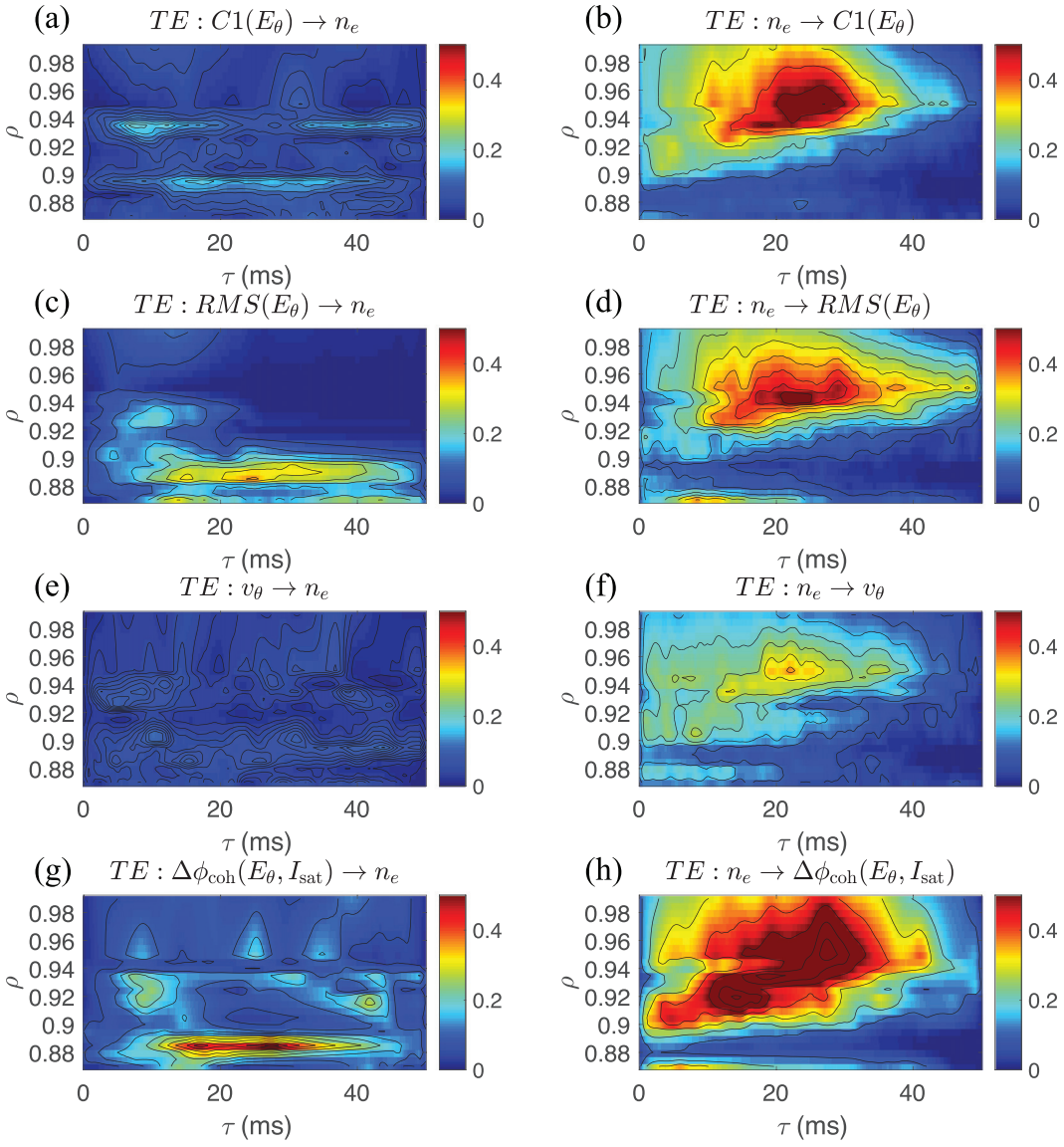

FIG. 5. Transfer entropy between the line average electron density $\overline{n_e}$ and several variables of interest, as indicated in the plot headings. Horizontal axes: time lag τ (ms). Vertical axes: probe position in terms of normalized radius, ρ.

vertical axis corresponds to the probe position, which was varied on a shot to shot basis.

Several things are immediately clear: (1) The TE values of the graphs $\overline{n_e} \rightarrow X$ are generally much larger than those of the graphs $X \rightarrow \overline{n_e}$, indicating that information flows from $\overline{n_e}$ to the other quantities, consistent with the idea that $\overline{n_e}$ acts as a control parameter. (2) Radial variation is significant. The largest values of TE are achieved around $\rho \simeq 0.95$–0.96, roughly where the transport barrier is formed.[22] (3) The time lags corresponding to the maxima of TE are $\tau \simeq 25$ ms, which is of the order of the transition time.

We draw attention to the fact that the values of TE are very high compared to the maximum value possible $[\log_2(3) \simeq 1.6]$. Interestingly, the impact of $\overline{n_e}$ on the cross phase $\Delta\phi_{\mathrm{coh}}(E_\theta, I_{\mathrm{sat}})$ occurs earlier for $\rho \simeq 0.91$ than for $\rho \simeq 0.96$ [cf., Fig. 5(h)]. This is consistent with Fig. 4(e), where the phase change is seen to propagate outward following the transition time.

Figure 6 shows the TE between several selected quantities of interest. One particular variable is seen to have a significant causal impact: RMS(E_θ), i.e., the turbulence level; it has a large impact on the cross phase $\Delta\phi_{\mathrm{coh}}(E_\theta, I_{\mathrm{sat}})$ [cf., Fig. 6(d)], significant impact on the intermittence, $C_1(E_\theta)$ [cf., Fig. 6(b)], and to a lesser degree on the poloidal phase velocity v_θ [Fig. 6(f)]. Here also, the influence appears to occur earlier at more inward positions of the probe.

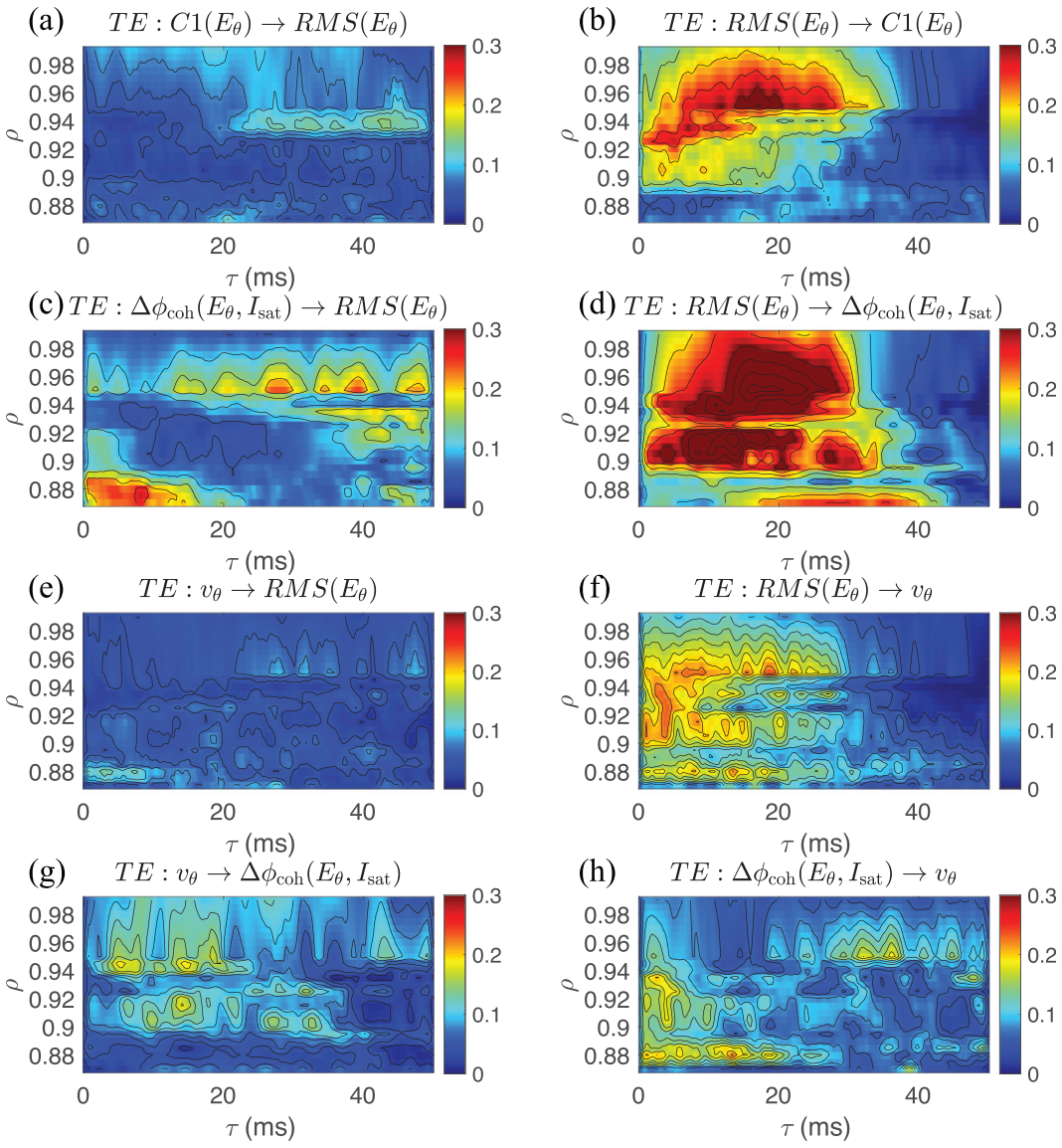

FIG. 6. Transfer entropy between several variables of interest, as indicated in the plot headings. Horizontal axes: time lag τ (ms). Vertical axes: probe position in terms of normalized radius, ρ.

V. DISCUSSION

The analysis performed here reveals the complexity of the dynamical interactions between turbulence and transport across the confinement transition. On the one hand, the plasma rapidly switches from electron to ion root conditions as the electric field is reversed.[23] On the other hand, the increase in the electron density modifies the intrinsic dynamics of the turbulence by modifying the driving gradients. These two mechanisms (background transport and turbulence) dynamically interact in a complex way.

We study the evolution of several key variables, in particular the cross phase between E_θ and I_{sat}, appearing in the turbulent particle flux, $\Gamma = \langle \tilde{E}_\theta \tilde{n} \rangle / B$, providing new information regarding the transition process. First, key variables are visualized on a spatiotemporal grid in the relevant plasma edge region. Second, several additional quantities are studied to facilitate further understanding, namely, the intermittence and the transfer entropy. Here, it should be noted that the e- to i-root transition itself, marked by the change of sign of v_θ and E_r, occurs fast, which does not allow extracting its impact from these analyses. However, it is possible to elucidate causal relations on the slower timescale of continuous variations across the transition, as exemplified in Fig. 1.

The line integrated density, $\overline{n_e}$, is the key control parameter for the transition. Increasing $\overline{n_e}$ implies a global increase in the density gradients, while the establishment of the edge transport barrier implies

a local increase in the density gradients, both of which increase the turbulence drive; cf. the impact on RMS(E_θ) in Fig. 5(d). It is interesting to note that this impact occurs first at inward positions and later at positions that are further outward.

The enhanced turbulence affects the cross phase $\Delta\phi_{\mathrm{coh}}(E_\theta, I_{\mathrm{sat}})$ [Fig. 6(d)] and causes $C_1(E_\theta)$ to drop [Figs. 4(c), 4(d) and 6(b)]. The latter implies that a dominant low-order helicity is growing (Fig. 2), which causes changes in v_θ via Reynolds stress [Fig. 6(f)]. The poloidal flow velocity v_θ is considered crucial for the actual transition.

The fact that $C_1(E_\theta)$ drops suggests that the sheared flow can at least in part be ascribed to the presence of low-order rational surfaces (e.g., $\iota = 5/3$ at $\rho \simeq 1$ and $\iota = 18/11$ at $\rho \simeq 0.86$).[17] This idea might explain why the various quantities respond earlier at positions close to the inner part of the observational domain, $\rho \simeq 0.86$ ($\iota = 18/11$): the transition would be initiated near that location. The interaction between turbulence and such dominant low-order modes, therefore, possibly plays a key role in the formation and maintenance of the sheared flow and the transport barrier.

The poloidal flow, v_θ, and cross phase, $\Delta\phi(E_\theta, I_{\mathrm{sat}})$, visualized in Figs. 4(e) and 4(f), respectively, appear to evolve in parallel. On physical grounds, the sheared flow (i.e., the shearing rate) is expected to be the key driving force of the change in the cross phase, even if the corresponding graphs of Fig. 6, the TE between v_θ and $\Delta\phi(E_\theta, I_{\mathrm{sat}})$, are not very impressive. It should be noted, though, that both v_θ and $\Delta\phi(E_\theta, I_{\mathrm{sat}})$ are the result of a certain level of numerical processing, which may obfuscate delicate causal relationships. In any case, the zone of maximum shearing rate [roughly, the light green band in Fig. 4(f)] is seen to propagate outwards prior to the consequential phase change. We note that the change in cross phase is very significant ($\gtrsim \pi/2$).

At the time of the transition, when v_θ changes sign, a short-lived, large amplitude zonal flow structure is observed (Fig. 1), characterized by a significant deviation of E_r from v_θ. This temporal behaviour is similar to what has been observed elsewhere.[27]

After the transition, the plasma is in a new state (the ion root) and is maintained in that state by neoclassical requirements (ambipolarity).[23] It is interesting to note that the changed cross phase is maintained at its new value (Fig. 1), associated with the new equilibrium profiles in the ion root state, in particular, the v_θ or flow profile.

VI. CONCLUSIONS

In this work, we have studied the spontaneous electron to ion root transition using Langmuir probe data in the plasma edge region, with both spatial and temporal resolution. The probe layout allowed studying a number of relevant quantities: turbulence amplitude [RMS(E_θ) and RMS(I_{sat})], E_r, E_θ, v_θ, $\Delta\phi(E_\theta, I_{\mathrm{sat}})$, as well as the intermittence $C_1(E_\theta)$ and $C_1(I_{\mathrm{sat}})$. The causal relation between the various quantities was studied using the transfer entropy.

It was found that the turbulence experiences significant simultaneous changes across the transition, as reflected by the evolution of all mentioned quantities (Fig. 1): The turbulence amplitude (RMS) and the cross phase ($\Delta\phi$) increase, while the intermittence (C_1) drops. The spatiotemporal evolution obtained by varying the probe position ($0.87 \leq \rho \leq 0.99$) in similar discharges (Fig. 4) shows, for example, that the cross phase $\Delta\phi(E_\theta, I_{\mathrm{sat}})$ changes first in inward positions and then propagates outward. The poloidal velocity v_θ also experiences such an outward propagating change.

Analysis with the transfer entropy reveals that the line average electron density $\overline{n_e}$ acts as a control parameter of the transition, presumably indirectly, via the local density gradient that acts as a turbulence drive. Note that the edge density gradient roughly increases by a factor of 2, as reported in Ref. 22. The time delay between the density change and the response of the plasma is approximately 25 ms. Again, the change is seen to propagate outward (Fig. 5). Finally, the transfer entropy between various relevant turbulent quantities was studied, showing that the main drive is the turbulence amplitude RMS(E_θ), which mainly impacts the intermittence $C_1(E_\theta)$ and the poloidal velocity v_θ.

ACKNOWLEDGMENTS

This work has been carried out within the framework of the EUROfusion Consortium and has received funding from the Euratom research and training programme 2014–2018 and 2019–2020 under Grant Agreement No. 633053 and project Y2018/NMT-4750 [PROMETEO-CM] Comunidad de Madrid. The views and opinions expressed herein do not necessarily reflect those of the European Commission. Research sponsored in part by the Ministerio de Ciencia, Innovación y Universidades of Spain under Project No. PGC2018-097279-B-I00. B.A.C. gratefully acknowledges support for the research from the DOE office of Fusion Energy under U. S. Department of Energy Contract No. DE-SC0018076.

DATA AVAILABILITY

The data that support the findings of this study are available from the corresponding author upon reasonable request.

REFERENCES

[1]J. Boedo, P. Terry, D. Gray, R. Ivanov, R. Conn, S. Jachmich, G. Van Oost, and TEXTOR Team, Phys. Rev. Lett. **84**, 2630 (2000).
[2]A. Ware, P. Terry, P. Diamond, and B. Carreras, Plasma Phys. Controlled Fusion **38**, 1343 (1996).
[3]D. A. Schaffner, T. A. Carter, G. D. Rossi, D. S. Guice, J. E. Maggs, S. Vincena, and B. Friedman, Phys. Rev. Lett. **109**, 135002 (2012).
[4]G. Birkenmeier, M. Ramisch, B. Schmid, and U. Stroth, Phys. Rev. Lett. **110**, 145004 (2013).
[5]T. Kobayashi, Nucl. Fusion **60**, 095001 (2020).
[6]J. Harris, J. Cantrell, T. Hender, B. Carreras, and R. Morris, Nucl. Fusion **25**, 623 (1985).
[7]C. Hidalgo *et al.*, Nucl. Fusion **45**, S266 (2005).
[8]B. van Milligen, T. Estrada, E. Ascasíbar, D. Tafalla, D. López-Bruna, A. López-Fraguas, J. Jiménez, I. García-Cortés, A. Dinklage, R. Fischer, and TJ-II Team, Rev. Sci. Instrum. **82**, 073503 (2011).
[9]B. van Milligen, J. Nicolau, L. García, B. Carreras, C. Hidalgo, and TJ-II Team, Nucl. Fusion **57**, 056028 (2017).
[10]C. Hidalgo, M. Pedrosa, E. Sánchez, B. Gonçalves, J. Alonso, E. Calderón, A. Chmyga, N. Dreval, L. Eliseev, T. Estrada, L. Krupnik, A. Melnikov, R. Orozco, J. de Pablos, and C. Silva, Plasma Phys. Controlled Fusion **48**, S169 (2006).
[11]B. van Milligen, T. Kalhoff, M. Pedrosa, and C. Hidalgo, Nucl. Fusion **48**, 115003 (2008).
[12]G. Grenfell, M. Spolaore, D. Abate, L. Carraro, L. Marrelli, I. Predebon, S. Spagnolo, M. Veranda, M. Agostini, B. Van Milligen, R. Cavazzana, L. Cordaro, G. De Masi, P. Franz, C. Hidalgo, E. Martines, B. Momo, M. Puiatti, P. Scarin, N. Vianello, B. Zaniol, and M. Zuin, Nucl. Fusion **60**, 126006 (2020).
[13]M. Pedrosa, C. Hidalgo, C. Silva, B. Carreras, D. Carralero, I. Calvo, and TJ-II Team, Contrib. Plasma Phys. **50**, 507 (2010).
[14]C. Ritz, E. Powers, T. Rhodes, R. Bengtson, K. Gentle, H. Lin, P. Phillips, A. Wootton, D. Brower, N. Luhmann, W. Peebles, P. Schoch, and R. Hickok, Rev. Sci. Instrum. **59**, 1739 (1988).
[15]C. Meneveau and K. Sreenivasan, Phys. Rev. Lett. **59**, 1424 (1987).

[16]C. Meneveau and K. Sreenivasan, J. Fluid Mech. **224**, 429 (1991).
[17]B. Carreras, L. García, J. Nicolau, B. van Milligen, U. Hoefel, M. Hirsch, and TJ-II and W7-X Teams, Plasma Phys. Controlled Fusion **62**, 025011 (2020).
[18]B. van Milligen, A. Melnikov, B. Carreras, L. Garcia, A. Kozachek, C. Hidalgo, J. de Pablos, P. Khabanov, L. Eliseev, and M. Drabinskij, Nucl. Fusion (to be published) (2021).
[19]B. van Milligen, G. Birkenmeier, M. Ramisch, T. Estrada, C. Hidalgo, and A. Alonso, Nucl. Fusion **54**, 023011 (2014).
[20]B. van Milligen, B. Carreras, L. García, and J. Nicolau, Entropy **21**, 148 (2019).
[21]M. Pedrosa, C. Silva, C. Hidalgo, B. Carreras, R. Orozco, D. Carralero, and TJ-II Team, Phys. Rev. Lett. **100**, 215003 (2008).
[22]B. van Milligen, M. Pedrosa, C. Hidalgo, B. Carreras, T. Estrada, J. Alonso, J. de Pablos, A. Melnikov, L. Krupnik, L. Eliseev, and S. Perfilov, Nucl. Fusion **51**, 113002 (2011).
[23]J. Velasco, J. Alonso, I. Calvo, and J. Arévalo, Phys. Rev. Lett. **109**, 135003 (2012).
[24]B. van Milligen, L. García, B. Carreras, M. Pedrosa, C. Hidalgo, J. Alonso, T. Estrada, and E. Ascasíbar, Nucl. Fusion **52**, 013006 (2011).
[25]B. van Milligen, T. Estrada, R. Jiménez-Gómez, A. Melnikov, C. Hidalgo, J. Fontdecaba, L. Krupnik, L. Eliseev, S. Perfilov, and TJ-II Team, Nucl. Fusion **51**, 013005 (2011).
[26]R. Balbín, C. Hidalgo, M. Pedrosa, I. García-Cortés, and J. Vega, Rev. Sci. Instrum. **63**, 4605 (1992).
[27]G. Grenfell, B. van Milligen, U. Losada, T. Estrada, B. Liu, C. Silva, M. Spolaore, and C. Hidalgo, Nucl. Fusion **60**, 014001 (2020).